Geometric interpretation of chaos in two-dimensional Hamiltonian systems

Henry E. Kandrup*
Department of Astronomy and Department of Physics, and Institute for Fundamental Theory, University of Florida, Gainesville, Florida 32611
(Received 7 March 1997)

This paper exploits the fact that Hamiltonian flows associated with a time-independent H can be viewed as geodesic flows in a curved manifold, so that the problem of stability and the onset of chaos hinge on properties of the curvature K_{ab} entering into the Jacobi equation. Attention focuses on ensembles of orbit segments evolved in representative two-dimensional potentials, examining how such properties as orbit type, values of short time Lyapunov exponents χ, complexities of Fourier spectra, and locations of initial conditions on a surface of section correlate with the mean value and dispersion, $\langle\widetilde{K}\rangle$ and $\sigma_{\widetilde{K}}$, of the (suitably rescaled) trace of K_{ab}. Most analyses of chaos in this context have explored the effects of negative curvature, which implies a divergence of nearby trajectories. The aim here is to exploit instead a point stressed recently by Pettini [Phys. Rev. E **47**, 828 (1993)], namely, that geodesics can be chaotic even if K is everywhere positive, chaos in this case arising as a parametric instability triggered by regular variations in K along the orbit. For ensembles of fixed energy, containing both regular and chaotic segments, simple patterns exist connecting $\sigma_{\widetilde{K}}$ for different segments both with each other and with the short time χ. Often, but not always, there is a nearly one-to-one correlation between $\langle\widetilde{K}\rangle$ and $\sigma_{\widetilde{K}}$, a plot of these two quantities approximating a simple curve. Overall χ varies smoothly along the curve, certain regions corresponding to regular and ''confined'' chaotic orbits where χ is especially small. Chaotic segments located furthest from the regular regions tend systematically to have the largest χ's. The values of $\langle\widetilde{K}\rangle$ and $\sigma_{\widetilde{K}}$ (and in some cases χ) for regular orbits also vary smoothly as a function of the ''distance'' from the chaotic phase space regions, as probed, e.g., by the location of the initial condition on a surface of section. Many of these observed properties can be understood qualitatively in terms of a one-dimensional Mathieu equation, in which parametric instability is introduced in the simplest possible way. [S1063-651X(97)06809-8]

PACS number(s): 05.45.+b, 03.20.+i, 02.40.−k

I. INTRODUCTION AND MOTIVATION

It is well known [1] that the flow associated with a time-independent Hamiltonian $H=\frac{1}{2}\delta^{ab}p_a p_b+V(x^a)$ can be reformulated as a geodesic flow in a curved, but conformally flat, manifold. Specifically, let

$$ds^2=W(x^a)\,\delta_{ab}dx^a dx^a, \tag{1}$$

where E is the conserved energy associated with the time-independent H and the conformal factor

$$W(x^a)=E-V(x^a) \tag{2}$$

is equal numerically to the kinetic energy associated with a trajectory at the point x^a. It then follows that, with the further identification

$$ds=\sqrt{2}W\,dt, \tag{3}$$

the geodesic equation for motion in the metric $g_{ab}=W\delta_{ab}$ is completely equivalent to the Hamilton equations

$$\frac{dx^a}{dt}=\frac{\partial H}{\partial p_a},\quad \frac{dp_a}{dt}=-\frac{\partial H}{\partial x^a}. \tag{4}$$

This implies that the confluence or divergence of nearby trajectories $x^a(s)$ and $[x+\xi]^a(s)$ is determined by the Jacobi equation, i.e., the equation of geodesic deviation, which takes the form

$$\frac{D^2\xi^a}{Ds^2}=-R^a{}_{bcd}u^b u^d\xi^c\equiv -K^a{}_c\xi^c, \tag{5}$$

where R_{abcd} is the Riemann tensor associated with g_{ab} and $D/Ds=u^a\nabla_a$ denotes a directional derivative along $u^a=dx^a/ds$. Linear stability or lack thereof for the trajectory $x^a(s)$ is thus related to R_{abcd} or, more precisely, to the curvature $K^a{}_c$. If, e.g., R_{abcd} is everywhere negative, so that $K^a{}_c$ always has one or more negative eigenvalues, the trajectory must be linearly unstable.

It would seem intuitive that, if the curvature of g_{ab} is everywhere negative, so that nearby trajectories always tend to diverge, every geodesic will behave in a fashion that is manifestly chaotic. If one assumes that the manifold is compact, so that trajectories are restricted to a region of finite volume, this intuition can be evaluated to a theorem. For example, geodesic flows on a compact manifold with constant negative curvature are necessarily K flows, where generic ensembles of initial conditions evolve towards a microcanonical distribution at a rate set by the magnitude of the curvature [2]. If the curvature is everywhere negative but not constant, the flow is more complex, but one can still infer [3]

*Electronic address: kandrup@astro.ufl.edu

a chaotic evolution towards a microcanonical distribution at a rate bounded from below by the least negative value of the curvature.

When the curvature is not everywhere negative, much less is known. Nevertheless, the preceding has motivated the expectation that, in many dynamical systems, chaos should be associated with (regions of) negative curvature. In particular, several authors (cf. [4,5]) have sought to use negative curvature to explain the fact that the gravitational N-body problem for a large number objects of comparable mass is chaotic in the sense that the evolution manifests an exponentially sensitive dependence on initial conditions.

However, as stressed recently by Pettini [6], not all chaos can be associated with negative curvature. In particular, one can have large measures of chaotic orbits even for systems and energies where K_{ab} is everywhere positive. In retrospect, this is easy to understand. Viewing the Jacobi equation as a matrix equation, one can solve at any given point in space to derive eigenvectors $\{\mathbf{X}_i\}$ and eigenvalues $\{\lambda_i\}$, each pair solving a linear equation of the form

$$\frac{D^2\mathbf{X}_i}{Ds^2} = -\lambda_i \mathbf{X}_i . \tag{6}$$

When the curvature is everywhere positive, $\lambda_i \geq 0$, so that the solutions are oscillatory rather than exponential. If the λ_i's were constant along the trajectory, one could thus infer stable oscillations. In general, however, the λ_i's are not constant, depending instead on the unperturbed $x^i(s)$ since R_{abcd} and u^a both change along the trajectory. It follows that, even assuming an everywhere positive curvature, Eq. (6) should be interpreted as an oscillator equation

$$\frac{D^2\mathbf{X}_i}{Ds^2} = -\Omega_i^2(s)\mathbf{X}_i . \tag{7}$$

The obvious point is that solutions to Eq. (7) can manifest a parametric instability.

Because the coordinates and velocity of a regular orbit are periodic, the frequency $\Omega(s)$ must also be periodic, so that Eq. (7) reduces to an oscillator equation with periodic modulation, e.g., a Hill equation. If the unperturbed geodesic is to be stable, so that it can exist as a regular orbit, it must be that solutions to this equation represent bounded oscillations, a condition that implies nontrivial restrictions on the time dependence of Ω. If these restrictions are not satisfied, the geodesic must instead correspond to a chaotic orbit.

As observed by Cerruti-Sola and Pettini [7], this intuition is particularly simple to implement for two-dimensional systems. In this case, $K^a{}_b$ corresponds to a symmetric 2×2 matrix, one eigenvalue of which is necessarily zero, corresponding to neutral stability with respect to infinitesimal translations along the orbit from $x^a(s)$ to $x^a(s+\delta s)$. It follows that, in interpreting the behavior of a small perturbation, it suffices to restrict attention to perturbations in the single direction orthogonal to the velocity u^a, so that one is reduced to a single scalar equation.

More explicitly, by exploiting the fact that, in two dimensions, the Riemann tensor has only one independent nonzero component, say $R^x{}_{yxy}$, it is easily seen that

$$K^a{}_b = \begin{pmatrix} R^x{}_{yxy}(u^y)^2 & -R^x{}_{yxy}u^x u^y \\ -R^x{}_{yxy}u^x u^y & R^x{}_{yxy}(u^x)^2 \end{pmatrix}, \tag{8}$$

from which it follows that there are two eigenvalues, namely, $\lambda = 0$ and $\lambda = R^x{}_{yxy}[(u^x)^2 + (u^y)^2] = K^x{}_x + K^y{}_y$. Transforming from u^a to the physical momentum p_a and recalling that W is equal numerically to the kinetic energy, the nonzero eigenvalue is

$$\lambda = R_{xyxy}/W^2, \tag{9}$$

where, explicitly,

$$R_{xyxy} = \frac{1}{2}\left[\frac{\partial^2 V}{2x^2} + \frac{\partial^2 V}{\partial y^2}\right] + \frac{1}{2W}\left[\left(\frac{\partial V}{\partial x}\right)^2 + \left(\frac{\partial V}{\partial y}\right)^2\right]. \tag{10}$$

The component of ξ^a orthogonal to u^a thus satisfies

$$\frac{d^2\xi_1}{ds^2} = -K\xi_1 = -\frac{1}{2}R\xi_1 , \tag{11}$$

where $K \equiv K^x{}_x + K^y{}_y$ and R denotes the scalar curvature. Alternatively, translating back into physical time t one finds (cf. [7])

$$\frac{d^2\xi_1}{dt^2} - \frac{1}{W}\frac{dW}{dt}\frac{d\xi_1}{dt} = -2R_{xyxy}\xi_1 = -W^2K\xi_1 . \tag{12}$$

Cerruti-Sola and Pettini [7] have studied representative orbits in one prototypical two-dimensional potential, namely, the Hénon-Heiles potential [8], demonstrating thereby that one can effect a translation between various orbital properties as viewed in the ordinary Hamiltonian language and as viewed in this geometric language. However, it is also useful to study the statistical properties of ensembles of orbit segments since this facilitates a search for bulk regularities connecting different properties of representative orbits. Thus, in particular, such an investigation can provide important information about how quantities like short time Lyapunov exponents $\chi(t)$ [9] correlate with properties of the curvature K_{ab} as evaluated along some orbit. This is of interest for chaotic orbits, where one knows that changing values of short time Lyapunov exponents can reflect phase space transport through cantori [10] and other topological obstructions [11] and/or the overall complexity of an orbit segment, as probed by its Fourier spectrum [12]. This is also useful for regular orbits where, for different initial conditions, the short time exponent $\chi(t)$ can converge towards the asymptotic Lyapunov exponent $\chi_\infty = \chi(t\to\infty)$ at very different rates. Indeed, for fixed time t the value of $\chi(t)$ for different regular orbits with the same energy E can vary by more than an order of magnitude.

Equations (11) and (12) might suggest that the natural quantity upon which to focus is K or W^2K. However, when realized as a function of W and its derivatives, both these quantities involve (cf. Eq. [10]) division by positive powers of W, which, for small values of W, can lead to skewed statistics for a finite sampling. For this reason, it was discovered that cleaner results were obtained by focusing on

$$\widetilde{K} \equiv W^3K = WR_{xyxy} . \tag{13}$$

Physically this combination arises if one introduces a new time coordinate τ satisfying $ds = W^{3/2} d\tau$, so that

$$\frac{d^2\xi_1}{d\tau^2} - \frac{3}{2W}\frac{dW}{d\tau}\frac{d\xi_1}{d\tau} = -W^3 K \xi_1 . \tag{14}$$

The fact that the statistical properties of $\widetilde{K} = W^3 K$ correlate very strongly with properties of the unperturbed orbit suggests that it is the coefficient of ξ_1, rather than its time derivative, that is responsible for much of the orbit's observed behavior.

The work described in this paper involved examining the quantity $\widetilde{K}$ as evaluated along different orbit segments, probing in particular values of the mean $\langle \widetilde{K} \rangle$ and the dispersion $\sigma_{\widetilde{K}}$. The resulting data were used to establish trends related to these quantities, including how different segments—both regular and chaotic—fit into the $\langle \widetilde{K} \rangle$-$\sigma_{\widetilde{K}}$ plane, and how the values assumed by these quantities depend on other orbital characteristics, e.g., on whether a regular orbit is a box or a loop or whether a chaotic segment looks nearly regular or particularly complex. Especially striking were correlations between $\langle \widetilde{K} \rangle$ or $\sigma_{\widetilde{K}}$ and the values of short time Lyapunov exponents $\chi(t)$ computed for the same segments. Given that the value of χ is strongly correlated with the overall complexity of the orbit, as probed by its Fourier spectrum [12], such correlations also connect statistical properties of $\widetilde{K}$ with the shape of the orbit, as viewed in configuration space.

As noted by Pettini (private communication), the preceedings justification for focusing $\widetilde{K} = W^3 K$, rather than $W^2 K$, is potentially suspect since, at least in principle, any nontrivial time reparametrization can significantly alter the stability properties of geodesics. Fortunately, however, there is another interpretation that may perhaps be more easily justified: computing the average of $W^2 K$ along a geodesic can be interpreted as involving a ratio of integrals $\int \sqrt{g}\, dx\, dy\, W^2 K / \int \sqrt{g}\, dx\, dy$, where g denotes the determinant of the metric g_{ij} and the integration extends over the regions of the manifold along which the geodesic moves. However, it follows from Eq. (2) that this reduces to $\int dx\, dy\, W^3 K / \int dx\, dy\, W$, and, to the extent that $\int dx\, dy\, W$ is approximately constant (as a consequence of virialization), one is effectively averaging the quantity $W^3 K$.

The results presented below derive from an analysis of orbit segments in two different representative two-dimensional potentials. The first of these,

$$V(x,y) = -(x^2+y^2) + \tfrac{1}{4}(x^2+y^2)^2 - \tfrac{1}{4}x^2 y^2, \tag{15}$$

corresponds to the so-called dihedral potential of Armbruster *et al.* [13], for one particular set of parameter values. The second,

$$V(x,y) = \tfrac{1}{2}(x^2+y^2) + x^2 y - \tfrac{1}{3}y^3 + \tfrac{1}{2}x^4 + x^2 y^2 + \tfrac{1}{2}y^4 + x^4 y + \tfrac{2}{3}x^2 y^3 - \tfrac{1}{3}y^5 + \tfrac{1}{5}x^6 + x^4 y^2 + \tfrac{1}{3}x^2 y^4 + \tfrac{11}{45}y^6, \tag{16}$$

represents the sixth order truncation of the Toda [14] lattice potential (recall that the Hénon-Heiles potential can be derived as the third order truncation of the Toda potential). These are very different qualitatively but, nevertheless, much of the observed behavior is very similar for orbit segments in both potentials. In the truncated Toda potential, $\widetilde{K}$ is always non-negative. However, for certain energies in the dihedral potential $\widetilde{K}$ can be negative along parts of some orbits, although $\widetilde{K}$ tends to be positive most (>75–$80\,\%$) of the time.

Ensembles of orbit segments with fixed energy E were generated by sampling the $E = \text{const}$ hypersurface and then evolving typically for a total time $t = 256$, this in units where a typical crossing time (i.e., the time required for an orbit to cross from one side of the potential to the other) $t_{\rm cr} \sim 1$–2. This is a reasonable time interval to consider because chaotic segments in these potentials tend to exhibit significant qualitative changes on a time scale $\sim (100$–$200) t_{\rm cr}$ [15]. However, it was verified that similar results are obtained for somewhat longer and shorter total times. In most cases, the initial ensemble was generated by setting $x = 0$, uniformly sampling the energetically allowed portions of the y-p_y plane, and then computing an initial $p_x > 0$ as a function of x, y, p_y, and E. The orbits were integrated using a fourth order Runge-Kutta scheme with a time step $\delta t = 10^{-4}$.

Strictly speaking, when extracting statistical properties of $\widetilde{K}$ it is most natural to analyze a time series that records relevant quantities at fixed intervals of geodesic time s, rather than at fixed intervals of ''physical'' time t, which is achieved most easily by solving the geodesic equation associated with $W\delta_{ab}$ rather than the original Hamilton equations. However, it was found that the basic correlations involving quantities like $\langle \widetilde{K} \rangle$ and $\sigma_{\widetilde{K}}$ were equally apparent for both sorts of time series. The discussion here focuses primarily on data recorded at fixed intervals δt. This has the advantage that the conclusions derived here for the dihedral and truncated Toda potentials can be easily tested for other potentials, without the inconvenience of explicitly reformulating the evolution as a geodesic flow.

Section II describes various trends and correlations observed in the numerical experiments, demonstrating in particular the existence of striking regularities connecting quantities like $\langle \widetilde{K} \rangle$, $\sigma_{\widetilde{K}}$, and χ, many of which can be interpreted in terms of other physical properties of the orbits. Section III summarizes the principal conclusions and then shows that, not surprisingly, many of these can in fact be understood in terms of a simple one-dimensional Mathieu equation.

II. OBSERVED CORRELATIONS AMONG $\langle \widetilde{K} \rangle$, $\sigma_{\widetilde{K}}$, AND χ

A. Correlations between $\langle \widetilde{K} \rangle$ and $\sigma_{\widetilde{K}}$

In most, albeit not all, cases, i.e., for most energies in both potentials, the values of the mean $\langle \widetilde{K} \rangle$ and the dispersion $\sigma_{\widetilde{K}}$ of different orbit segments are strongly correlated. Rather than filling a large portion of the $\langle \widetilde{K} \rangle$-$\sigma_{\widetilde{K}}$ plane, the orbit segments tend to fall, at least approximately, along a single curve. For the dihedral potential, this curve is typically quite thin; for the truncated Toda potential, it can be significantly thicker. Moreover, this curve is typically characterized overall by a negative slope, so that orbits with larger $\langle \widetilde{K} \rangle$ have smaller $\sigma_{\widetilde{K}}$.

Figures 1 and 2 exhibit plots of $\sigma_{\widetilde{K}}$ as a function of $\langle \widetilde{K} \rangle$ for several different energies in, respectively, the dihedral and truncated Toda potentials. Figures 1(d)–1(h) and Figs. 2(c) and 2(d), each characterized by a single curve, per-

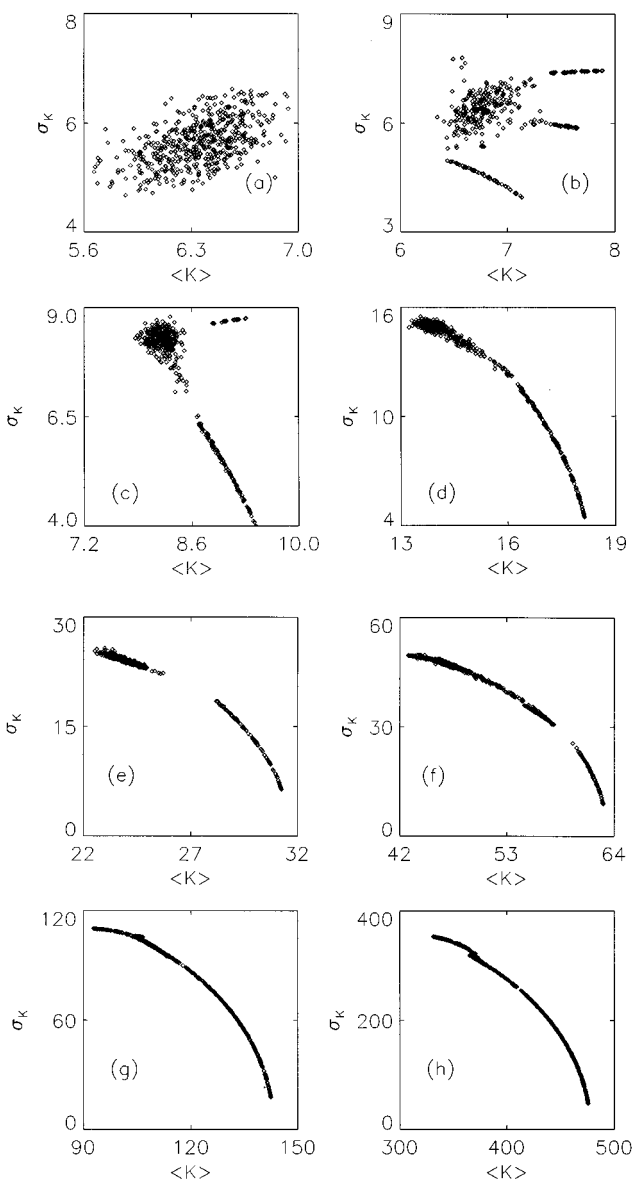

FIG. 1. The mean $\langle\widetilde{K}\rangle$ and dispersion $\sigma_{\widetilde{K}}$ for orbit ensembles with eight different energies E evolved in the dihedral potential for a total time $t=256$. (a) $E=-0.05$. (b) $E=0.05$. (c) $E=0.25$. (d) $E=1.0$. (e) $E=2.0$. (f) $E=4.0$. (g) $E=8.0$. (h) $E=20.0$.

haps with one or more intermittent gaps [as in Figs. 1(e) and 1(f)] or a slight ''wiggle'' [as in Fig. 1(h)] represent typical behavior. The fact, manifest visually, that the values of $\langle\widetilde{K}\rangle$ and $\sigma_{\widetilde{K}}$ are strongly correlated can be quantified by computing the rank correlation $\mathcal{R}(\langle\widetilde{K}\rangle,-\sigma_{\widetilde{K}})$. For these typical cases in the dihedral potential, the correlation between $\langle\widetilde{K}\rangle$ and $-\sigma_{\widetilde{K}}$ is usually very strong, $\mathcal{R}>0.98$ or more. For the truncated Toda potential, the correlation is often somewhat weaker, $\mathcal{R}(\langle\widetilde{K}\rangle,-\sigma_{\widetilde{K}})\sim 0.9-0.95$, but still significant.

This sort of correlation between $\langle\widetilde{K}\rangle$ and $\sigma_{\widetilde{K}}$, seemingly suggestive of ordered behavior, is perhaps not surprising for regular orbits, where the motion is multiply periodic. Thus, e.g., it is easy to envision a sequence of regular box or loop orbits characterized by smoothly varying values of $\langle\widetilde{K}\rangle$ or $\sigma_{\widetilde{K}}$. However, such correlations might seem less expected

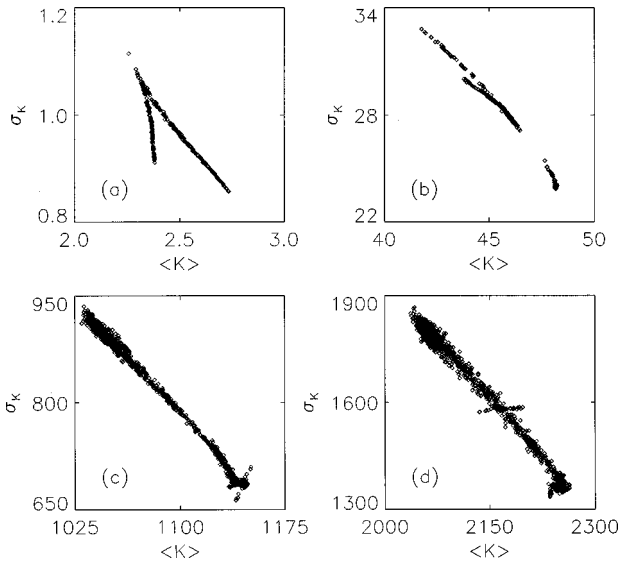

FIG. 2. The mean $\langle\widetilde{K}\rangle$ and dispersion $\sigma_{\widetilde{K}}$ for orbit ensembles with four different energies E evolved in the truncated Toda potential for a total time $t=256$. (a) $E=0.5$. (b) $E=3.0$. (c) $E=20.0$. (d) $E=30.0$.

for chaotic orbits where the motion is aperiodic. It is therefore significant that, when viewed in such a $\langle\widetilde{K}\rangle$-$\sigma_{\widetilde{K}}$ plot, regular orbits need not stand out in any obvious way. Consider, e.g., the orbit ensemble with $E=4.0$ used to generate Fig. 1(f). Here one finds that there are three distinct types of regular orbits, a large number of orbits with $59<\langle\widetilde{K}\rangle<63$ and $9<\sigma_{\widetilde{K}}<26$, a large number of orbits with $54<\langle\widetilde{K}\rangle<57$ and $33<\sigma_{\widetilde{K}}<36$, and a small number of orbits with $43<\langle\widetilde{K}\rangle<45$ and $49<\sigma_{\widetilde{K}}<50$. It is clear that all the points below the gap in Fig. 1(f) are associated with regular orbits, and a careful examination of the data points allows one to distinguish minute differences between the locations of the regular and chaotic orbits in the intermediate regime, $54<\langle\widetilde{K}\rangle<57$ and $33<\sigma_{\widetilde{K}}<36$. However, it is evident that, overall, the regular and chaotic orbits coexist along a relatively narrow curve [16].

This can be associated tentatively with the fact that, even though chaotic orbits are intrinsically aperiodic, finite chaotic segments often manifest a fair amount of regularity. Thus, e.g., as discussed more carefully below, one often observes that the power spectra, $|x(\omega)|$ and $|y(\omega)|$, for a chaotic segment typically appear visually to be constructed from ''pieces'' appropriate for a small number of regular orbits [12,17]. This interpretation is especially natural given the recognition that the most striking exception to the simple pattern described hitherto is associated with very low energies in the dihedral potential, where few, if any, regular orbits exist.

Figure 1(a), a seemingly structureless set of points completely different from the lines observed in the remaining panels of Figs. 1 and 2, derives from an ensemble of segments with $E=-0.05$, an energy where a sampling of nearly 1000 different initial conditions yielded only chaotic orbits. At slightly higher energies, regular orbits begin to appear and, unlike the chaotic orbits, they seem concentrated largely along lines in the $\langle\widetilde{K}\rangle$-$\sigma_{\widetilde{K}}$ plane. Thus, e.g., as illustrated in Fig. 1(b), for $E=+0.05$ there are four different types of regular orbits, three of these associated with the three con-

spicuous lines and the fourth associated with the largest values of $\sigma_{\tilde{K}}$ above the central chaotic region. As the energy is raised to yet higher values, the regular families associated with the two upper lines eventually disappear, so that, e.g., as illustrated in Fig. 1(d) for $E=1.0$, all the orbits fit approximately onto a single curve, with the chaotic orbits at high $\sigma_{\tilde{K}}$ and the regular orbits at low $\sigma_{\tilde{K}}$. When the energy is raised to a higher value, $E\sim 3$, other regular orbit families appear, leading eventually to the aforementioned behavior at $E=4.0$.

The observed behavior at low energies in the truncated Toda potential is quite different, presumably reflecting the fact that, in this case, at very low energies there is no global stochasticity. For energies $E<5.0$ or so, all the orbits present, both regular and chaotic, fit into two distinct lines in the $\langle\tilde{K}\rangle$-$\sigma_{\tilde{K}}$ plane. Consider, e.g., the energy $E=0.5$ exhibited in Fig. 1(a). Here most of the upper line is occupied by loop orbits, which manifest a discrete $2\pi/3$ rotation symmetry, whereas the lower line is occupied completely by box and banana orbits that break this symmetry. There are only a very few chaotic orbits at this energy, and all of them fit at the high $\sigma_{\tilde{K}}$ end of the upper line. As the energy increases, the lower line eventually shrinks and merges into the upper line, so that, ultimately, different families of regular orbits coexist with chaotic orbits along a single thickened curve.

B. Correlations between curvature and $\chi(t)$

Ordinary Lyapunov exponents χ, which [18] probe the average instability of some trajectory in an asymptotic $t\rightarrow\infty$ limit, manifest a fundamental distinction between regular and chaotic orbits. For regular orbits all the Lyapunov exponents vanish identically, whereas chaotic orbits have at least one χ that is positive. Orbits in a D-dimensional system have $2D$ distinct Lyapunov exponents, these corresponding to perturbations in $2D$ independent phase space directions. For a time-independent Hamiltonian system, two of these exponents must vanish [reflecting neutral stability with respect to perturbations that translate an orbit from $x^a(t)$ to $x^a(t+\delta t)$ and to perturbations orthogonal to the constant energy surface] and the remaining exponents must come in pairs, $\pm\chi$. It follows that, for two-dimensional Hamiltonian systems, the only fundamental distinction is between regular orbits, for which all the χ's vanish, and chaotic orbits, which have one exponent $\chi>0$.

However, one can also introduce short time Lyapunov exponents $\chi(t)$, which provide information about the average instability of orbit segments over a finite interval. Thus, in particular, for any phase space perturbation δZ, one can define [9]

$$\chi(t)\equiv\lim_{t\rightarrow\infty}\lim_{\delta Z(0)\rightarrow 0}\frac{1}{t}\ln\left[\frac{\|\delta Z(t)\|}{\|\delta Z(0)\|}\right], \tag{17}$$

where $\|\cdot\|$ represents a suitable norm. For a generic initial perturbation, this $\chi(t)$ will converge towards the largest Lyapunov exponent in the limit $t\rightarrow\infty$, independent of the detailed choice of norm. By contrast, at finite times the computed $\chi(t)$ will depend on both the initial perturbation and the choice of norm. Suppose, however, that $\|\cdot\|$ is taken as the natural L^2 phase space norm, i.e., $\|\delta Z\|^2=(\delta x)^2+(\delta y)^2+(\delta p_x)^2+(\delta p_y)^2$. In this case, one knows that the computed $\chi(t)$ will be insensitive to the detailed choice of initial perturbation for times $t\gg 1/\chi(t)$.

It follows that, for chaotic segments integrated in the dihedral and truncated Toda potentials for times as long as $t=256$, the computed $\chi(t)$ is nearly independent of the initial δZ. However, as described below the values of $\chi(t)$ computed for regular orbits can, and in certain cases do, exhibit a significant dependence on δZ. For the experiments described in this paper, $\chi(t)$ was computed [18] by introducing a small perturbation of magnitude $\|\delta Z\|=10^{-10}$, evolving both unperturbed and perturbed initial conditions, and periodically renormalizing the perturbation to an amplitude $\|\delta Z\|=10^{-10}$ at intervals $\Delta t=10$. Unless stated otherwise, the initial perturbation was taken as $\delta Z=\delta x=10^{-10}$.

The objective here is to show that, for both regular and chaotic orbit segments, strong correlations exist between the value of the short time $\chi(t)$ and such properties of the curvature as $\langle\tilde{K}\rangle$ and $\sigma_{\tilde{K}}$. Because the quantities $\langle\tilde{K}\rangle$ and $\sigma_{\tilde{K}}$ are themselves correlated, it would seem equally reasonable to look for correlations between $\chi(t)$ and either $\langle\tilde{K}\rangle$ or $\sigma_{\tilde{K}}$ (or any combination of these two quantities). For specificity, most of the discussion will focus on correlations between $\sigma_{\tilde{K}}$ and $\chi(t)$, although several figures exhibit examples of correlations between $\langle\tilde{K}\rangle$ and $\chi(t)$. Figures 3 and 4 exhibit plots of χ as a function of $\sigma_{\tilde{K}}$, generated respectively for the dihedral and truncated Toda potentials for the same ensembles used to generate Figs. 1 and 2.

Consider first the case of orbit ensembles evolved in the dihedral potential. For $E=-0.05$, where there are few if any regular orbits, a plot of χ as a function of $\sigma_{\tilde{K}}$ shows little obvious structure: all that one sees is a seemingly random scattering of points at values of χ well separated from $\chi=0$. However, as E increases, one begins to observe the existence of regular regions, which correspond to ranges of $\sigma_{\tilde{K}}$ where, for some segments, χ assumes values much smaller than the values associated with chaotic segments. Thus, e.g., as illustrated in Fig. 3(b), for $E=0.05$ one observes an extended low $\sigma_{\tilde{K}}$ band that corresponds to one regular line in Fig. 1(b), a collection of points near $\sigma_{\tilde{K}}=6.0$ corresponding to the second line, another collection near $\sigma_{\tilde{K}}=7.4$ corresponding to the third line, and a small number of small χ points near $\sigma_{\tilde{K}}=7.8$ corresponding to the high $\sigma_{\tilde{K}}$ points in Fig. 1(b).

For $E>0.2$ or so, a simpler pattern emerges that includes only two types of regular orbits; they are concentrated at especially low and high values of $\sigma_{\tilde{K}}$ (or, equivalently, high and low values of $\langle\tilde{K}\rangle$). At somewhat higher energies, the high $\sigma_{\tilde{K}}$ family disappears, only to be replaced by a new regular family concentrated at intermediate values of $\sigma_{\tilde{K}}$. At yet higher energies, one sees two large regular regions, concentrated at the largest and smallest values of $\sigma_{\tilde{K}}$, along with some intermediate regions with small χ's that are associated with nearly vertical lines in the $\sigma_{\tilde{K}}$-χ plane. Viewed in a surface of section, the low $\sigma_{\tilde{K}}$ regular region corresponds to a large island of loop orbits; the high $\sigma_{\tilde{K}}$ region corresponds to a large island of box orbits. The regular orbits associated with the vertical lines correspond to smaller islands embedded in the stochastic sea. This structure appears to persist to very high energies.

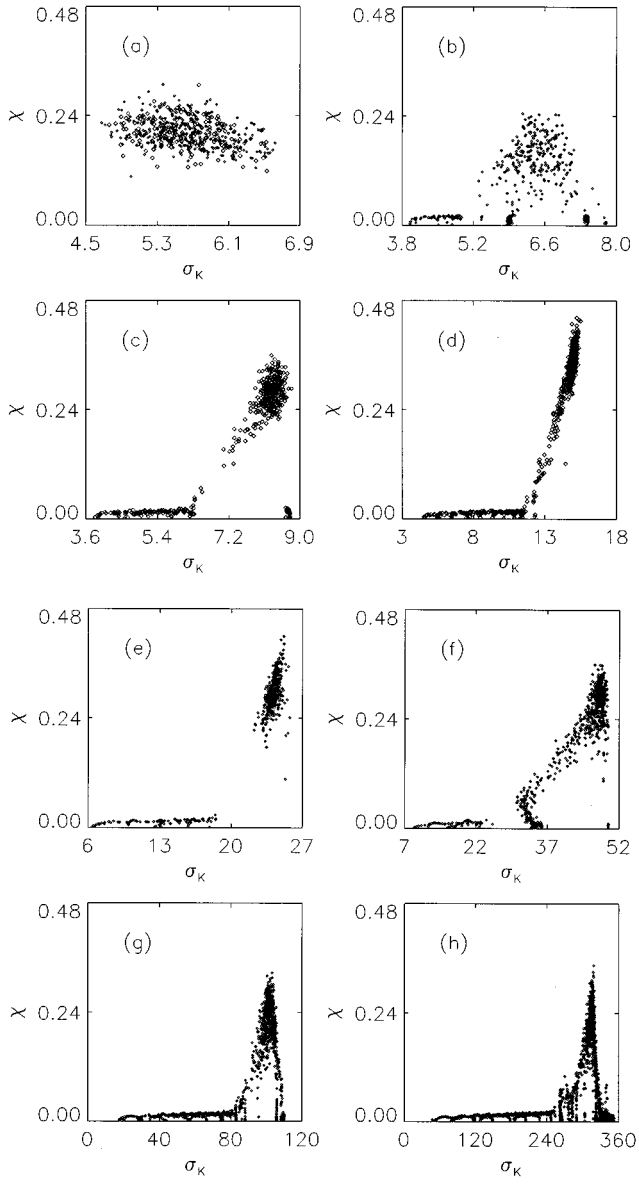

FIG. 3. The short time Lyapunov exponent χ plotted as a function of $\sigma_{\widetilde{K}}$ for the same orbit ensembles as in Fig. 1.

For these relatively high energies, $E>6.0$ or so, a plot of χ as a function of $\sigma_{\widetilde{K}}$ or $\langle\widetilde{K}\rangle$ exhibits several striking regularities. One significant point, well illustrated for $E=10.0$ in Fig. 5, is that the transition from regularity to chaos observed at low and high values of $\sigma_{\widetilde{K}}$ (or high and low values of $\langle\widetilde{K}\rangle$) is relatively abrupt. Thus, e.g., the small $\sigma_{\widetilde{K}}$, large $\langle\widetilde{K}\rangle$ loop orbits can be viewed as a sequence beginning at $\sigma_{\widetilde{K}}\approx 22$ that terminates at a value of $\sigma_{\widetilde{K}}\approx 112$, whereas the large $\sigma_{\widetilde{K}}$, small $\langle\widetilde{K}\rangle$ boxes can be viewed as a sequence extending upwards from $\sigma\langle\widetilde{K}\rangle\approx 124$ and terminating at a value $\langle\widetilde{K}\rangle \approx 135$. The chaotic segments situated near the boundary with the outer regular regions tend typically to be ''confined'' or ''sticky'' chaotic orbits [19] trapped near the regular regions by cantori [10] that, oftentimes, only escape to travel throughout the remainder of the stochastic sea on a time scale $t>256$. It is also apparent from Fig. 5 that (even away from the boundaries) chaotic segments with values of $\sigma_{\widetilde{K}}$ furthest from the high and low $\sigma_{\widetilde{K}}$ regular regions tend systematically to have larger χ's than do chaotic segments with values of $\sigma_{\widetilde{K}}$ closer to the outer regular regions. The net result is a curve that, viewed broadly, resembles a Greek Λ.

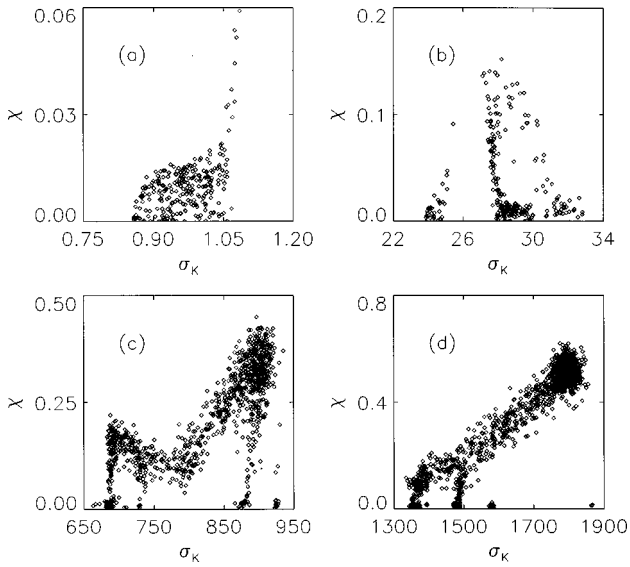

FIG. 4. The short time Lyapunov exponent χ plotted as a function of $\sigma_{\widetilde{K}}$ for the same orbit ensembles as in Fig. 2.

The overall shape of the $\sigma_{\widetilde{K}}$-χ curve in the regular region depends on the choice of the initial seed δZ used in computing the short time $\chi(t)$. If, as in Figs. 5(a) and 5(b), one computes χ from a seed $\delta Z=\delta x$, it is apparent that the segments with values of $\sigma_{\widetilde{K}}$ (or $\langle\widetilde{K}\rangle$) closest to the central chaotic region, $112<\sigma_{\widetilde{K}}<142$ or so, tend overall to have larger values of χ than do orbits with values of $\sigma_{\widetilde{K}}$ further from this chaotic region. However, if χ is generated instead from a seed with a significant component in one of the other three phase space directions, this trend is significantly diminished. This is illustrated in Figs. 5(c) and 5(d), which exhibit χ's generated for the same initial conditions from a seed $\delta Z=\delta y$. This difference presumably reflects the fact that, since the initial conditions were sampled from an $x=0$ surface of section, a perturbation $\delta Z=\delta x$ tends to be more nearly aligned along a direction of neutral stability, namely, translation from $\mathbf{x}(t)$ to $\mathbf{x}(t+\delta t)$, than do perturbations with a nonzero δy.

At lower energies, where the high $\sigma_{\widetilde{K}}$ region is absent or not well developed, the right side of the Λ is missing. However, one still observes that chaotic segments with $\sigma_{\widetilde{K}}$ closer to the regular region tend to have smaller values of χ than do chaotic segments far from the regular regions; and, at least for a seed $\delta Z\approx\delta x$, that regular orbits closer to the chaotic region tend to have larger values of χ.

One obvious complication associated with the common Λ pattern, well illustrated in Fig. 5, is the presence of one or more nearly vertical lines in the chaotic region, extending from very low to relatively high values of χ. The lowest values of χ seem too small to be associated with chaotic segments, but the upper values seem too large to be associated with regular orbits. In fact, these lines contain two different classes of orbits, namely, regular orbits, for which $\chi(t)$ eventually decays to zero, and confined chaotic orbits, trapped temporarily near a small regular island, which eventually escape through one or more cantori to travel unim-

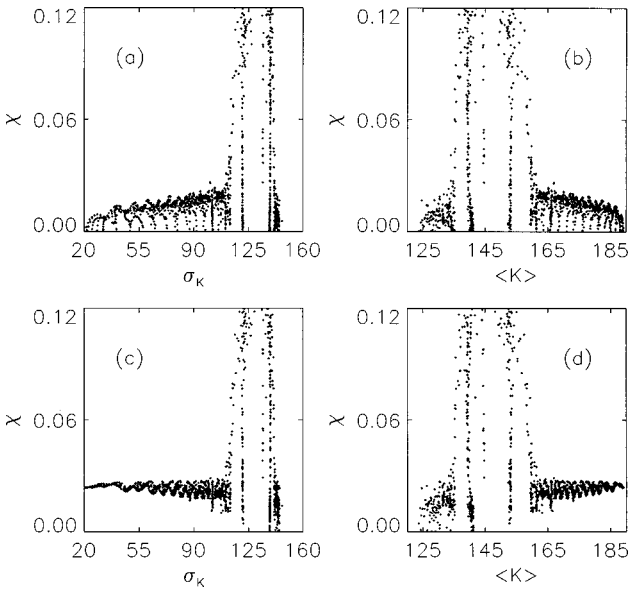

FIG. 5. (a) Short time Lyapunov exponents $\chi(t)$, generated with an initial perturbation $\delta x = 10^{-10}$ and plotted as functions of $\sigma_{\tilde{K}}$ for an ensemble of orbit segments with $E = 10.0$ evolved in the dihedral potential for a total time $t = 256$. Only values of $\chi < 0.16$ are shown. (b) The same $\chi(t)$'s plotted as a function of $\langle \tilde{K} \rangle$. (c) The analog of (a), generated for the same ensemble, but now allowing for an initial perturbation $\delta y = 10^{-10}$. (d) The analog of (b), generated for an initial perturbation $\delta y = 10^{-10}$.

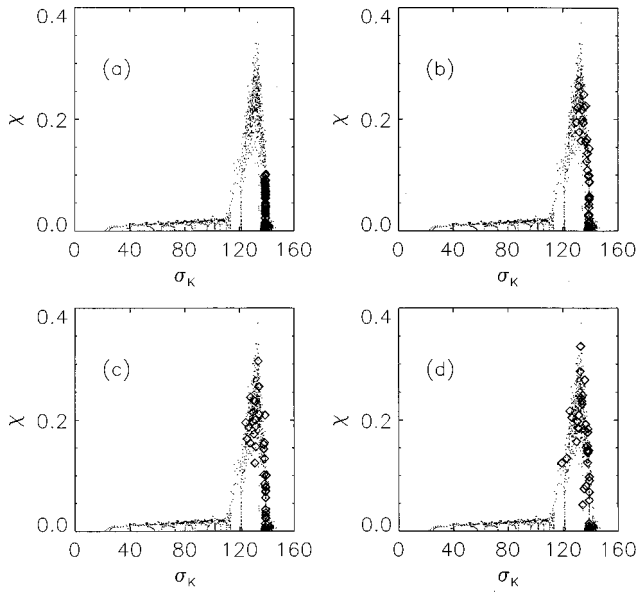

FIG. 6. The evolution of regular and confined chaotic orbits for $E = 10.0$ in the dihedral potential, with χ plotted as a function of $\sigma_{\tilde{K}}$. The dots represent analogs of Fig. 3, with a total integration time $t = 256$. The diamonds represent the same initial conditions analyzed over different time intervals. (a) $0 < t < 256$. (b) $256 < t < 512$. (c) $512 < t < 768$. (d) $768 < t < 1024$.

peded through the stochastic sea. Viewed in configuration space, the regular orbits corresponding to these lines correspond to periodic orbits confined to an annulus or a ''figure-eight-shaped'' region. The confined chaotic orbits correspond to aperiodic orbits that, for a long time, are trapped in almost the same region (whence follows the fact that they have nearly the same $\langle \tilde{K} \rangle$ and $\sigma_{\tilde{K}}$ as do the regular orbits), but eventually escape to probe the remaining chaotic phase space regions.

Evidence for these assertions is provided in Fig. 6, which summarizes an investigation of the longer time evolution of the initial conditions that led to the near vertical line in Fig. 5(b) at $\sigma_{\tilde{K}} \approx 139$. A random sampling of 1261 initial conditions with $E = 10.0$ evolved for a total time $\Delta t = 256$ led to 81 segments with $138 < \sigma_{\tilde{K}} < 140$ and $\chi(\Delta t) < 0.1$. These 81 initial conditions were subsequently integrated for a significantly longer time, $t = 8 \times 256$, with $\chi(t)$ recorded at regular intervals, and the resulting orbits partitioned into 8 segments of length $\Delta t = 256$, for which values $\sigma_{\tilde{K}}$ and $\langle \tilde{K} \rangle$ were computed. The recorded values of $\chi(t)$ were then analyzed to extract short time Lyapunov exponents for successive intervals of length $\Delta t = 256$, the exponent for the segment extending from $t_k = k\Delta t$ to $t_k + \Delta t$ being defined via the obvious relation (cf. [12])

$$\chi(\Delta t_k) = \frac{(t_k + \Delta t)\chi(t_k + \Delta t) - t_k \chi(t_k)}{\Delta t}. \qquad (18)$$

The tiny dots in all four panels of Fig. 6 exhibit the values of χ and $\sigma_{\tilde{K}}$ generated for the original ensemble of 1261 orbits evolved for a time $t = 256$. The diamonds in Fig. 6(a) highlight the 81 segments concentrated initially along the line near $\sigma_{\tilde{K}} = 139$. The diamonds in Fig. 6(b) show the values of χ and $\sigma_{\tilde{K}}$ derived from the same 81 initial conditions for the period $256 < t < 512$. Figures 6(c) and 6(d) extend the results to later intervals $512 < t < 768$ and $768 < t < 1024$. It is clear that, as time elapses, the larger χ diamonds escape from the line and move to other portions of the chaotic regions, whereas the smaller χ diamonds evolve closer to $\chi = 0$.

The other complication common to the Λ pattern is the existence of smaller scale structures in the regular regions. As noted already, for short time exponents generated from a seed δZ directed nearly in the x direction, many or most regular segments fit along a curve with χ decreasing as one moves away from the central chaotic region to much larger or smaller values of $\sigma_{\tilde{K}}$. Alternatively, for more generic choices of δZ, a plot of χ as a function of $\sigma_{\tilde{K}}$ exhibits an upper envelope that is more nearly independent of $\sigma_{\tilde{K}}$. However, in each case this upper curve is not the whole story.

As illustrated in Figs. 5(c) and 5(d), for generic values of δZ the low $\sigma_{\tilde{K}}$ loop orbits exhibit two additional features, namely, (1) small scale oscillations in the $\sigma_{\tilde{K}}$-χ or $\langle \tilde{K} \rangle$-$\chi$ plane, and (2) an excess probability of finding segments with especially low values of χ *closer to*, rather than further from, the central chaotic region. Alternatively, as illustrated in Figs. 5(a) and 5(b), for δz oriented more nearly in the x direction one can identify various ''subfamilies'' of regular orbits which, for a fixed value of $\sigma_{\tilde{K}}$, tend to have much smaller values of χ than other regular orbits with (nearly) the same value of $\sigma_{\tilde{K}}$. Thus, e.g., if one focuses on a fixed interval of values of $\sigma_{\tilde{K}}$ and compares regular orbits with larger values of χ that fall along the upper line with regular orbits with smaller values of χ, he or she finds typically that there is a relatively clear cut difference between the two sets of orbits, as probed by the detailed shapes of their power spectra or, in some cases, by the overall shape of the orbit. In

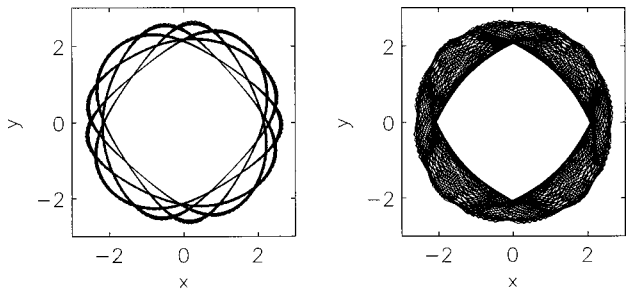

FIG. 7. Two orbits with $E=10.0$ evolved in the dihedral potential for a time $t=256$. (a) An orbit with $\langle\tilde{K}\rangle=183.4$, $\sigma_{\tilde{K}}=56.4$, $Q=\sigma_{\tilde{K}}/\langle\tilde{K}\rangle=0.308$, and $\chi=0.0051$. (b) An orbit with $\langle\tilde{K}\rangle=181.6$, $\sigma_{\tilde{K}}=62.7$, $Q=0.345$, and $\chi=0.0116$.

many cases, the regular orbits that have smaller values of χ tend to be ''simpler'' or ''more regular'' in appearance. This is illustrated in Fig. 7, which exhibits two representative regular orbits extracted from the interval $51.0<\sigma_{\tilde{K}}<58.0$. Figure 7(a) shows a typical low-χ orbit, whereas Fig. 7(b) shows a typical orbit lying along the upper curve. It is obvious that the higher χ orbit is (nearly) space filling within an annulus, whereas the lower orbit exhibits more structure.

The detailed patterns relating χ to $\sigma_{\tilde{K}}$ are different for initial conditions evolved in the truncated Toda potential, but the data still admit to a similar interpretation. At relative low energies, $E\sim 2-8$, one sees patterns qualitatively similar to those observed for $E>6$ or so in the dihedral potential. Alternatively, for somewhat higher energies, $E>25$ or so, one sees instead a pattern reminiscent of those observed at relatively low energies in the dihedral potential where, in the absence of a significant population of large $\sigma_{\tilde{K}}$ box orbits, one observes simply that, for chaotic segments, larger $\sigma_{\tilde{K}}$ correlates with larger χ. Superficially, the behavior for $E=20.0$, illustrated in Fig. 4(c), might seem quite different from what is observed in the dihedral potential since here the chaotic segments with the smallest values of χ are those furthest from the regular regions. However, when placed in an appropriate context this behavior is not surprising. At energies slightly above $E=20.0$, this low χ chaotic region merges into a relatively large regular island, which is well established by $E=25.0$. For $E=30.0$, one sees three large islands at low $\sigma_{\tilde{K}}$, the two corresponding to the lowest values of $\sigma_{\tilde{K}}$ very similar qualitatively to the islands for $E=10.0$ in the dihedral potential associated with the two vertical lines.

C. Curvature and complexity

The preceding shows that there is a strong correlation between the overall stability or instability of an orbit segment, as probed by the value of a short time Lyapunov exponent $\chi(t)$, and the values of $\langle\tilde{K}\rangle$ and $\sigma_{\tilde{K}}$ associated with that segment. However, earlier work [12] has shown that, for chaotic segments, there also exists a strong, nearly linear, correlation between $\chi(t)$ and the *complexity* of the segment, as probed by the form of its Fourier spectrum. One thus anticipates that there should exist correlations between $\langle\tilde{K}\rangle$ or $\sigma_{\tilde{K}}$ and the complexity of the segment.

As discussed more carefully in Ref. [12], $n(k)$, the complexity of an orbit segment at threshold k, can be defined in the following way. Given the values of the configuration space coordinates, say x and y, at fixed time intervals Δt, sampled, e.g., $\sim$5–10 times per crossing time, compute the power spectra, $|x(\omega)|$ and $|y(\omega)|$ in the usual way [20]. Next determine the minimum number of frequencies, $n_x(k)$ and $n_y(k)$, required respectively to capture a fixed fraction k of the x and y powers. The total complexity is then defined as

$$n(k)=n_x(k)+n_y(k). \tag{19}$$

This notion of complexity is motivated by the idea that ''comparatively regular'' segments have most of their power concentrated at or near a few special frequencies, whereas ''wildly chaotic'' segments have spectra with significantly broader band power. Experience with ensembles of orbits evolved in several different potentials has indicated that values $k\sim 0.9-0.95$ yield relative complexities in good agreement with subjective impressions based on visual inspection of segments in the x-y plane. The results described in this paper were derived from integrations where coordinates were recorded at fixed intervals $\Delta t=0.125$ for a total time $t=256$, leading to 2048 points and hence a Fourier series with 2048 frequencies.

As stated already, for orbit segments in both the dihedral and truncated Toda potentials, as well as for other systems [12], there is a strong, nearly linear correlation between $\chi(t)$ and quantities such as $n(0.9)$ or $n(0.95)$. For ensembles where χ and $n(k)$ both assume a broad range of values, the rank correlation typically assumes a value $\mathcal{R}(\chi,n(k))>0.85-0.9$. If, alternatively, most of the segments are concentrated in the same part of the χ-$n(k)$ plane, $\mathcal{R}$ can be smaller but still remains appreciable.

This correlation can be understood intuitively in terms of the fact that chaotic orbit segments often appear visually to be comprised of ''pieces'' of various regular orbits that exist at the same energy [16]. Consider, e.g., orbits with $E=10.0$ in the dihedral potential. Here one finds that chaotic segments with values of $\sigma_{\tilde{K}}$ near those appropriate for the two large regular regions tend overall to look more regular, and to have smaller complexities, than segments located at values of $\sigma_{\tilde{K}}$ further from the regular regions. Moreover, chaotic segments near the low $\sigma_{\tilde{K}}$ regular region tend to look ''loopy'' and to have power spectra dominated by features appropriate for the loop orbits that exist at small $\sigma_{\tilde{K}}$; and similarly, chaotic segments near the high $\sigma_{\tilde{K}}$ regular region tend to look ''boxy'' and to have spectra similar to the high $\sigma_{\tilde{K}}$ box orbits.

The degree to which a quantity like $n(0.9)$ correlates with χ, both in itself and in relation to other quantities like $\langle\tilde{K}\rangle$ or $\sigma_{\tilde{K}}$, can be gauged from Fig. 8, which exhibits data generated in the dihedral potential for $E=10.0$ and $E=1.0$. The two left panels exhibit plots of χ as functions of $\langle\tilde{K}\rangle$, whereas the two right panels plot $n(0.9)$ as a function $\langle\tilde{K}\rangle$. It is clear that, at least in the chaotic regions, the plots of χ and $n(0.9)$ exhibit the same basic features, although the plots of $n(0.9)$ seem more ''blurred.''

There is, however, a significant difference for the regular orbits. Plots of $n(0.9)$ [or $n(0.95)$] as a function of $\sigma_{\tilde{K}}$ or $\langle\tilde{K}\rangle$ exhibit large systematic oscillations not manifested in the plots of χ, whereas the small scale structures present in

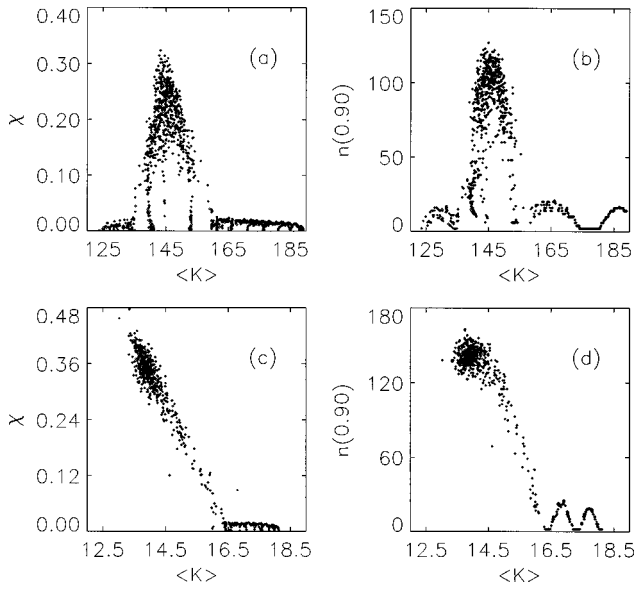

FIG. 8. (a) The short time exponent χ plotted as a function of $\langle \tilde{K} \rangle$ for a collection of orbits with $E=10.0$ evolved in the dihedral potential for a total time $t=256$. (b) The complexity $n(0.9)$ plotted as a function of $\langle \tilde{K} \rangle$ for the same set of segments. (c) The analog of (a) for a collection of segments with $E=1.0$. (d) The analog of (b) for the segments of (c).

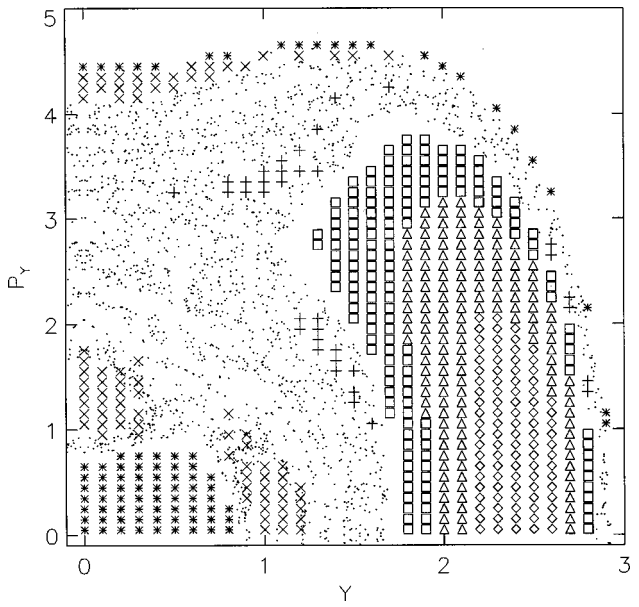

FIG. 9. An x-p_x surface of section for $E=10.0$ in the dihedral potential. The dots derive from a single unconfined chaotic orbit evolved for 2000 intersections. The remaining points represent some of the initial conditions used to generate Figs. 5 and 6. Diamonds represent loop orbits with $\sigma_{\tilde{K}}<72.0$. Triangles represent loop orbits with $72.0<\sigma_{\tilde{K}}<90.0$. Squares represent loop orbits with $90.0<\sigma_{\tilde{K}}<110.0$. Stars represent box orbits with $\sigma_{\tilde{K}}>141.0$. Pluses represent points along the near-vertical line with $120.0<\sigma_{\tilde{K}}<122$ and $\chi<0.08$. Crosses represent points along the line with $138.0<\sigma_{\tilde{K}}<140.0$ and $\chi<0.1$.

the plots of χ (cf. Fig. 5) are absent in plots of $n(0.9)$. Consider, e.g., $E=10.0$. Here all the segments at large $\langle \tilde{K} \rangle$ are regular loops, but the loops near $\langle \tilde{K} \rangle = 175$ are clearly special in that $n(0.9)$ assumes values that are particularly small. This reflects the fact that, in this region, peaks in the spectra $|x(\omega)|$ and $|y(\omega)|$ are much sharper than at somewhat larger and smaller values of $\langle \tilde{K} \rangle$.

This is a finite sampling effect, reflecting the fact that the orbit's segments were integrated for a relatively short time $t=256$. If the total time t is changed, but data are still recorded and analyzed at 2048 equally spaced intervals, one finds that, as would be expected, the values of $\langle \tilde{K} \rangle$ and $\sigma_{\tilde{K}}$ computed for regular segments remain essentially unchanged. By contrast, however, the details of the oscillations can be altered significantly. Thus, e.g., for $E=1.0$ the location of the dip near $\langle \tilde{K} \rangle = 17.5$ will move and other minima can appear. Moreover, one observes that, as t increases, the computed complexities decrease and the amplitudes of the oscillations damp.

One final correlation remains to be stated. To say that a regular orbit is close to the chaotic region is a statement about *both* its location (say) in the $\sigma_{\tilde{K}}$-χ plane *and* its actual location in configuration space, as probed, e.g., by a surface of section. For example, orbits in the large regular regions with values of $\langle \tilde{K} \rangle$ and $\sigma_{\tilde{K}}$ further from the central chaotic region tend systematically to lie closer to the center of a regular island than do regular segments with values of $\langle \tilde{K} \rangle$ and $\sigma_{\tilde{K}}$ closer to the central chaotic region. Similarly, the vertical lines associated with regular and confined chaotic orbits are associated with smaller regular islands embedded in the stochastic sea.

These facts are illustrated in Fig. 9. Here the small dots represent successive sections generated from a single ''unconfined'' chaotic initial condition that systematically avoids the phase space regions near the two large regular islands. The remaining symbols represent different initial conditions corresponding to regular and ''confined'' chaotic orbits generated from a uniform sampling of the y-p_y plane. The smaller of the two large islands, located near $y=p_y=0$ and populated with stars, corresponds to box orbits. The larger, displaced from $y=0$, corresponds instead to loop orbits. Here the initial conditions were binned into three classes. The diamonds represent segments with $\sigma_{\tilde{K}}$ assuming particularly small values, whereas the squares represent values of $\sigma_{\tilde{K}}$ especially close to the chaotic region. The triangles correspond to intermediate values. The remaining pluses and crosses represent initial conditions that led to the two nearly vertical lines exhibited in Fig. 5.

III. SUMMARY AND INTERPRETATION

Several general trends emerge from the experiments described in the preceding section. Most striking and fundamental, perhaps, is the fact that, for an ensemble of orbit segments of fixed energy E, a plot of the dispersion $\sigma_{\tilde{K}}$ as a function of the mean $\langle \tilde{K} \rangle$ usually assumes a very simple form. In general, regular and chaotic segments appear to coexist along a single curve in the $\langle \tilde{K} \rangle$-$\sigma_{\tilde{K}}$ plane, although for both potentials one sees more complicated structures at very low energies. The fact that chaotic segments fit along a single curve indicates that, even though they are aperiodic, they still exhibit significant statistical regularities.

Plots of the short time Lyapunov exponent $\chi(t)$ as a function of $\langle \tilde{K} \rangle$ or $\sigma_{\tilde{K}}$ also exhibit simple, distinctive patterns.

For example, one find that, largely independent of the initial perturbation δZ used in calculating χ, chaotic segments with values of $\langle \widetilde{K} \rangle$ (or $\sigma_{\widetilde{K}}$) far from the regions associated with regular orbits tend to have larger values of $\chi(t)$ than do chaotic segments with values of $\langle \widetilde{K} \rangle$ (or $\sigma_{\widetilde{K}}$) nearer the regular regions. For regular orbits, the computed values of $\chi(t)$, and hence any correlations with $\langle \widetilde{K} \rangle$ or $\sigma_{\widetilde{K}}$, depend more sensitively on the initial perturbation. For most initial perturbations, it seems that, overall, the typical $\chi(t)$ is nearly independent of $\langle \widetilde{K} \rangle$ and $\sigma_{\widetilde{K}}$. However, for some classes of perturbations one finds instead that segments with values of $\langle \widetilde{K} \rangle$ (or $\sigma_{\widetilde{K}}$) further from the chaotic regions tend to have smaller values of χ than do regular segments with values closer to the chaotic region.

The correlations between $\chi(t)$ and $\langle \widetilde{K} \rangle$ (or $\sigma_{\widetilde{K}}$) observed for chaotic orbits are very similar to the observed correlations between the complexity $n(k)$ and $\langle \widetilde{K} \rangle$ (or $\sigma_{\widetilde{K}}$). This reflects the fact that chaotic segments with values of $\langle \widetilde{K} \rangle$ and $\sigma_{\widetilde{K}}$ closer to the regular regions tend to look more regular and, consequently, to have less complex Fourier spectra than do orbits with values further from the regular region.

One other common feature, observed for both complexities and short time exponents, is the presence of one or more nearly vertical lines in (say) the $\sigma_{\widetilde{K}}$-χ or $\sigma_{\widetilde{K}}$-$n(k)$ plane. These are comprised of two distinct types of segments, namely, segments of regular orbits trapped forever in an island of stability by invariant KAM tori and ''confined'' chaotic orbits, trapped temporarily by cantori in a similar configuration space region which, however, eventually diffuse through the cantori to probe the remaining portions of the chaotic sea.

Many of these qualitative features can be reproduced in a much simpler context, where the linearized scalar Jacobi equation (11) is replaced by a linear Matthieu equation of the form [21]

$$\frac{d^2\xi_1}{dt^2} = (\omega + \gamma \sin t)\xi_1, \tag{20}$$

where ω and γ play the roles, respectively, of $\langle \widetilde{K} \rangle$ and $\sigma_{\widetilde{K}}$.

If one studies solutions to Eq. (20) as a function of ω and γ (or, by analogy, $\langle \widetilde{K} \rangle$ and $\sigma_{\widetilde{K}}$) he or she finds that the ω-γ pane is partitioned into a large number of disjoint regions, corresponding respectively to ''regular'' and ''chaotic'' orbits. In the regular regions, it is apparent that, in the $t \to \infty$ limit, the analog of the ordinary short time Lyapunov exponent,

$$\chi(t) = \frac{1}{t} \ln\left[\frac{\|\delta Z(t)\|}{\|\delta Z(0)\|}\right], \tag{21}$$

with $\|\delta Z\|^2 = |\xi_1|^2 + |\xi_1|^2$, eventually converges towards zero. Alternatively, in the chaotic regions $\chi(t)$ converges towards a time-independent positive value. It follows that a generic curve passing through the ω-γ (or $\langle \widetilde{K} \rangle$-$\sigma_{\widetilde{K}}$) plane, analogous to the curves exhibited in Figs. 1 and 2, will include both regular and chaotic regions with sharp transitions between the two.

For values of ω and γ far from the chaotic portions of the curve, one finds typically that, for reasonably large t, the computed value of χ is relatively insensitive to the detailed perturbation and to the exact values of ω and γ. However, for values of ω and γ closer to the chaotic regions, more complicated patterns can arise. Viewed in an asymptotic $t \to \infty$ limit, the transition from regular to chaotic is abrupt. However, the transition is smooth in the sense that, when evaluated for some finite time t, the short time $\chi(t)$ computed for ''chaotic'' values of ω and γ close to the regular regions is typically smaller than the $\chi(t)$ computed for values that are further from the regular region. This is consistent with the fact, manifested in Figs. 3–5 that orbits with values of $\langle \widetilde{K} \rangle$ and $\sigma_{\widetilde{K}}$ further from the regular regions tend to have larger short time Lyapunov exponents. Given this observation, it is also easy to understand (cf. Fig. 6) why, for ''sticky'' chaotic segments confined near regular regions by cantori, the computed $\chi(t)$ tends to be smaller than for other chaotic segments that travel further from the regular regions.

A detailed discussion of the sense in which the onset of chaos can be understood in terms of a more general Hill equation has been presented by Cerruti-Sola and Pettini [7] in the context of their analysis of individual orbits.

The work described in this paper has established the existence of a strong correlation between such geometric properties of chaotic orbit segments as $\langle \widetilde{K} \rangle$ and $\sigma_{\widetilde{K}}$ and the short time Lyapunov exponent χ. However, one might expect that this local, short time analyses could also be extended to establish a global connection between moments of $\widetilde{K}$, as defined along an infinite chaotic geodesic, and the ordinary Lyapunov exponent χ_∞, as defined in a $t \to \infty$ limit. Casetti *et al.* [22] have shown that, at least for systems with a large number N of degrees of freedom, such a connection does indeed exist. Specifically, by assuming that the curvature experienced by a chaotic orbit can be approximated as a random process, characterized by a mean $\langle K \rangle$ and a dispersion σ_K, they obtained an analytic approximation to the largest Lyapunov exponent which, in at least some cases, agrees extremely well with numerical computations.

It would seem unlikely that such a simple Gaussian approximation, which these authors motivate in the large-N limit, will work well for the very special case $N=2$. However, one might nevertheless hope that, in some fashion, the value of the positive Lyapunov exponent for a two-dimensional system can again be related to the moments of K or $\widetilde{K}$ evaluated along the chaotic orbit. This possibility is currently under investigation.

ACKNOWLEDGMENTS

I am grateful to Haywood Smith and, especially, Marco Pettini, for helpful comments on preliminary versions of this paper. This research was supported in part by the National Science Foundation Grant No. PHY92-03333. Some of the preliminary analysis was performed by Barbara L. Eckstein, who has been supported by NASA through the Florida Space Grant Consortium. Some of the computations were facilitated by computer time made available through the Research Computing Initiative at the Northeast Regional Data Center (Florida) by arrangement with IBM.

[1] Cf. L. D. Landau and E. M. Lifshitz, *Mechanics* (Pergamon, Oxford, 1960); V. I. Arnold, *Mathematical Methods of Classical Mechanics* (Springer, Berlin, 1978).
[2] Cf. E. Hopf, Trans. Am. Math. Soc. **39**, 229 (1936).
[3] D. V. Anosov, Trudy Mat. Inst. Steklov **90**, 1 (1967).
[4] V. G. Gurzadyan and G. K. Savvidy, Astron. Astrophys. **160**, 203 (1986).
[5] H. E. Kandrup, Physica A **169**, 73 (1990); Astrophys. J. **364**, 420 (1990).
[6] M. Pettini, Phys. Rev. E **47**, 828 (1993).
[7] M. Cerruti-Sola and M. Pettini, Phys. Rev. E **53**, 179 (1995).
[8] M. Hénon and C. Heiles, Astron. J. **69**, 73 (1964).
[9] Cf. P. Grassberger, R. Badii, and A. Politi, J. Stat. Phys. **51**, 135 (1988).
[10] Cf. J. N. Mather, Topology **21**, 457 (1982); R. S. MacKay, J. D. Meiss, and I. C. Percival, Phys. Rev. Lett. **52**, 697 (1984).
[11] M. E. Mahon, R. A. Abernathy, B. O. Bradley, and H. E. Kandrup, Mon. Not. R. Astron. Soc. **275**, 443 (1995).
[12] H. E. Kandrup, B. L. Eckstein, and B. O. Bradley, Astron. Astrophys. **320**, 65 (1997).
[13] D. Armbruster, J. Guckenheimer, and S. Kim, Phys. Lett. A **140**, 416 (1989).
[14] M. Toda, J. Phys. Soc. Jpn. **22**, 431 (1967).
[15] This is of special interest physically given the fact that, for a system like a galaxy, $100t_{cr}$ corresponds to a period of time comparable to the age of the Universe.
[16] In certain cases, e.g., for chaotic orbits trapped by cantori near regular islands, it is not easy to determine whether or not a given segment is in fact chaotic. To make precise determination in such potentially ambiguous cases, the segment was integrated for significantly longer times $t=2048$ to see whether the computed short time Lyapunov exponent $\chi(t)$ eventually begins to increase and/or whether, in configuration space, the segment eventually moves away from the regular island. When even such longer time integrations were inconclusive, the orbits were reintegrated in the presence of very weak additive white noise since [cf. S. Habib, H. E. Kandrup, and M. E. Mahon, Phys. Rev. E **53**, 5473 (1996); Astrophys. J. **480**, 155 (1997)] such perturbations tend to decrease dramatically the time scale on which chaotic orbits diffuse through cantori without allowing regular orbits to breach true KAM tori.
[17] H. E. Kandrup and B. L. Eckstein, Ann. (N.Y.) Acad. Sci. **808**, 139 (1997).
[18] Cf. G. Bennetin, L. Galgani, and J.-M. Strelcyn, Phys. Rev. A **14**, 2338 (1976).
[19] Cf. G. Contopoulos, Astron. J. **76**, 147 (1971) or R. S. Shirts and W. P. Reinhart, J. Chem. Phys. **77**, 5204 (1982).
[20] Cf. W. H. Press, B. P. Flannery, S. A. Teukolsky, and W. T. Vetterling, *Numerical Recipes*, 2nd ed. (Cambridge University Press, Cambridge, 1992).
[21] Cf. E. T. Whittaker and G. N. Watson, *A Course of Modern Analysis* (Cambridge University Press, Cambridge, 1965).
[22] L. Casetti, C. Clementi, and M. Pettini, Phys. Rev. E **54**, 5969 (1996).